Atmos. Chem. Phys. Discuss., 10, 14387–14415, 2010
www.atmos-chem-phys-discuss.net/10/14387/2010/
doi:10.5194/acpd-10-14387-2010
© Author(s) 2010. CC Attribution 3.0 License.

Atmospheric Chemistry and Physics Discussions

This discussion paper is/has been under review for the journal Atmospheric Chemistry and Physics (ACP). Please refer to the corresponding final paper in ACP if available.

Components of near-surface energy balance derived from satellite soundings – Part 1: Net available energy

A. Jarvis[1], K. Mallick[1], G. Wohlfahrt[2], C. Gough[3], T. Hirano[4], G. Kiely[5], A. Miyata[6], and S. Yamamoto[7]

[1]Atmospheric Sciences, Lancaster Environment Centre, Lancaster University, LA1 4YQ, UK
[2]Ecosystem Research and Landscape Ecology, University of Innsbruck, Innsbruck, 6020, Austria
[3]Department of Biology, Virginia Commonwealth University, Richmond, VA 23284-2012, USA
[4]Division of Environmental Resources, Research Faculty of Agriculture, Hokkaido University, Hokkaido, Japan
[5]Hydrometeorology Research Group, Department of Civil and Environmental Engineering, University College Cork, Ireland
[6]National Institute for Agro-Environmental Sciences, Tsukuba, Japan

[7]Graduate School of Environmental Science, Okayama University Tsushimanaka 3-1-1, Okayama 700-8530, Japan

Received: 24 March 2010 – Accepted: 23 May 2010 – Published: 9 June 2010

Correspondence to: K. Mallick (k.mallick@lancaster.ac.uk)

Published by Copernicus Publications on behalf of the European Geosciences Union.

ACPD
10, 14387–14415, 2010

Abstract

This paper introduces a method for recovering global fields of near-surface net available energy (the sum of the sensible and latent heat flux or the difference between the net radiation and surface heat accumulation) using satellite visible and infra-red products derived from the AIRS (Atmospheric Infrared Sounder) and MODIS (MOderate Resolution Imaging Spectroradiometer) platforms. The method focuses on first specifying net surface radiation by considering its various shortwave and longwave components. This was then used in a surface energy balance equation in conjunction with satellite day-night surface temperature difference to derive 12 h discrete time estimates of surface system heat capacity and heat accumulation, leading directly to a retrieval for surface net available energy. Both net radiation and net available energy estimates were evaluated against ground truth data taken from 30 terrestrial tower sites affiliated to the FLUXNET network covering 7 different biome classes. This revealed a relatively good agreement between the satellite and tower data, with a pooled root mean square deviation of 98 and 72 $\mathrm{W\,m^{-2}}$ for net radiation and net available energy, respectively, with little bias particularly for the net available energy.

1 Introduction

An important manifestation of climate change is widespread alterations to the composition of the energy balance at the Earth's surface. Given the importance of being able to predict the consequences of climate change, both measurement and modelling of the components of surface energy balance attract significant attention from a broad range of related scientific disciplines. Two such disciplines are hydrology and meteorology, which share a common interest in resolving the balance between sensible, H, and latent, λE, heat fluxes over a broad range of spatial and temporal scales.

Net available energy, Φ, is a core variable used to predict the magnitude of H and

ACPD
10, 14387–14415, 2010

λE given it is defined as the sum of these two fluxes (Wright et al., 1992),

$$\Phi = \lambda E + H \quad (1)$$

The utility of this definition arises from being able to also specify Φ as the difference between the net broadband radiation, R_N, and the rate of heat accumulation, G, below the plain across which R_N is specified,

$$\Phi = R_N - G \quad (2)$$

Given R_N is routinely measured using net radiometers this affords an opportunity to specify Φ and hence either H or λE. For example, in modelling studies λE is invariably specified as a function of Φ using now ubiquitous functions such as those of Penman (1948) for open water or Monteith (1965) for land surfaces. Despite being the rate of change of a heat stock, in terrestrial environments G is often interpreted as the "ground heat flux" and attempts to measure this using heat flux plates are commonplace (Mayocchi and Bristow, 1995; Sauer and Horton, 2005). These measurements prove somewhat less reliable than R_N due to greater spatial heterogeneity in ground heat uptake (Gao et al., 1998) allied to the fact that significant heat capacity resides in other elements of the land surface. As a result, G proves problematic in surface energy balance studies and is either ignored (Foken et al., 2006) despite being significant under a broad range of conditions (Santanello and Friedl, 2003), or treated somewhat superficially (Choudhury, 1987).

The arrival of satellite retrievals for many of the components of R_N has opened up opportunities to develop large scale estimates of this variable and hence λE (Batra et al., 2006; Mu et al., 2007). For example, retrievals for the components of R_N have been available through the International Satellite Cloud Climatology Project (ISCCP) (Pinker and Laszlo, 1992); the Earth Radiation Budget Experiment (ERBE); Clouds and Earth's Radiant Energy System (CERES) on board of the NASA Earth Observing System (EOS) and Tropical Rainfall Measuring Mission (TRMM) satellites (Wielicki et al., 1998). Several studies have reported the estimation of R_N using a combination

ACPD
10, 14387–14415, 2010

of MODIS (MOderate Resolution Imaging Spectroradiometer) atmospheric and land products over USA, China, and India (Bisht et al., 2005; Cai et al., 2007; Mallick et al., 2009) or NOAA-14 (National Oceanic and Atmospheric Administration) data over the Tibetan Plateau (Ma et al., 2002).

Unfortunately, in the absence of direct observations of G at spatial scales and coverage of satellite R_N, retrievals for Φ have had to rely on the parameterisation of G using surface temperature, albedo and vegetation index information (Bastiaanssen et al., 1998; Batra et al., 2006) or by assigning some fixed proportion of R_N (Choudhury, 1987; Humes et al., 1994) in satellite-based surface energy balance models (Mecikalski et al., 1999). But studies by Kustas et al. (1993) and recently Hsieh et al. (2009) demonstrated that G is, by definition, a highly dynamic quantity, and that the ratio G/R_N can range anywhere from 0.05 to 0.50 depending on the time of day, soil moisture and thermal properties, and vegetation density. Therefore, methods that are able to provide defensible estimates of G in conjunction with R_N in order to give Φ directly from satellite data without having to rely unduly on any offline calibration would clearly be of great benefit to this area. In this paper we present a method for retrieving R_N and Φ based on exploiting both satellite radiance data and day-night surface temperature difference. Taking advantage of the extensive network of terrestrial eddy covariance tower sites (Baldocchi et al., 2001) which record direct measurements of R_N, H and λE, we use these to derive independent non-radiative estimates of Φ in order to critically evaluate our satellite estimates of this quantity.

2 Methodology

2.1 Net radiation

The approach for estimating R_N uses the Atmospheric Infrared Sounder (AIRS) radiation products, although we have also made use of the MODIS surface reflectance and solar zenith angle products where necessary. R_N is generated by considering the

ACPD
10, 14387–14415, 2010

following balance between net shortwave (R_{NS}) and longwave (R_{NL}) radiation.

$$R_N = R_{NS} + R_{NL} = (1-\alpha)R_S + R_{L\downarrow} - R_{L\uparrow} \quad (3)$$

where α is the surface albedo and $R_{L\downarrow}$ and $R_{L\uparrow}$ are the downwelling and upwelling thermal radiative fluxes (all fluxes specified in $W\,m^{-2}$). Our chosen reference level for R_N is the near surface given this corresponds to the flux-based tower estimates we used in the evaluation. Therefore, surface R_S was estimated from its top-of-atmosphere clear sky counterpart R_{S0} and AIRS cloud cover fraction (f) following Hildebrandt et al. (2007),

$$R_S = (1-f)\tau_A R_{S0} \quad (4)$$

where τ_A is the clear sky transmissivity of the atmosphere which we assume is 0.75 (Cano et al., 1986; Thornton and Running, 1999; Hildebrandt et al., 2007). The terrestrial surface albedo was generated using the MODIS Aqua-Terra surface reflectances r_i following Liang et al. (1999),

$$\alpha = \sum_{i=1}^{N} p_i r_i + 0.0036 \quad (5)$$

where r_i are the mid-point reflectances within the 0.62–0.67; 0.841–0.876; 0.459–0.479; 0.545–0.565; 1.230–1.250; 1.628–1.653; and 2.105–2.155 µm wavelength bands and p_i are the weightings for each wavelength bands taken as p_i=(0.3973; 0.2382; 0.3489; −0.2655; 0.1604; −0.0138; 0.0682) (Liang et al., 1999). The albedo of ocean varies according to the cosine of solar zenith angle (Jin et al., 2004). In the present case, a constant albedo of 0.04 was assumed for oceans given the satellite radiances are nadir.

Clearly, many of the longwave components of the radiative balance are very closely related to the raw IR radiances being measured by AIRS. Given these are not in the public domain we have attempted to recover them as follows, although in future we

ACPD
10, 14387–14415, 2010

would anticipate using the raw IR radiances more directly if possible. R_{NL} was calculated as,

$$R_{NL} = R_{L\downarrow} - R_{L\uparrow} = \varepsilon_C \varepsilon_S \sigma T_C^4 - \varepsilon_S \sigma T_S^4 \quad (6)$$

where σ is the Stefan-Boltzmann constant (5.67×10^{-8} W m^{-2} K^{-4}), T_C is the columnar air temperature, and ε_C and ε_S are the column and surface emissivity, respectively. Among the different schemes for calculating ε_C we have used that proposed by Prata (1996) given this appears to be the most reliable (Bisht et al., 2005). This scheme uses AIRS total precipitable water (ξ) information to estimate ε_C as,

$$\varepsilon_C = 1 - (1 + \xi) e^{-(1.2+3\xi)^{0.5}} \quad (7)$$

The columnar air temperature T_C in Eq. (6) is taken as the average of the 2 m and 1000 hPa pressure level AIRS temperatures in an attempt to reflect a weighting toward the lower troposphere when specifying $R_{L\downarrow}$. T_S and ε_S are taken directly from the AIRS skin temperature and surface emissivity products.

2.2 Surface heat capacity, ground heat flux and net available energy

The definition of G stems from consideration of the non-steady state surface energy balance,

$$c \frac{dT_S(t)}{dt} = R_N(t) - \lambda E(t) - H(t) = G(t) \quad (8)$$

where c is the aggregate surface system heat capacity. The AIRS sounder platform samples twice daily at 01:30 and 13:30 LT. Despite being somewhat coarse, taking a discrete time, backward difference approximation of Eq. (8) with a sample interval $\Delta t = 12$ h equivalent to that of the AIRS pass gives,

$$\Delta T_s(t) = b_1 R_N(t) + b_2 \quad (9)$$

ACPD
10, 14387–14415, 2010

where ΔT_s is the day–night surface temperature change, $b_1 = \Delta t/c$ and $b_2 = -\Phi(t)\Delta t/c$. If we assume that the system is approximately in equilibrium over a 24 h cycle, and that at 01:30 LT $\Phi \approx 0$ (Tamai et al., 1998), then this gives the following simultaneous equations:

$$\Delta T_S(13{:}30\text{LT}) = b_1 R_N(13{:}30\text{LT}) + b_2 \quad (10a)$$

$$-\Delta T_S(13{:}30\text{LT}) = b_1 R_N(01{:}30\text{LT}) \quad (10b)$$

which can be solved analytically to derive b_1 and b_2 and hence Φ and c for each grid cell in the AIRS global array.

Clearly Eq. (10) is a coarse approximation of Eq. (8) and hence potentially suffers from a number of deficiencies. Firstly, diurnal symmetry in ΔT_s is only appropriate when one considers weekly or monthly average behaviour, and that there are no additional heat losses or gains to/from stores beyond the domain defined by the single heat capacity c. In this study we will be looking at monthly average behaviour because AIRS only gives partial global coverage on the daily timescale due to both cloud effects and the non-overlapping swath width of the sensor. Interactions with additional long term heat stores is an issue in systems such as the oceans where there can be a persistent heat loss/gains to/from deeper water over timescales of weeks to months, although relative to the diurnal fluctuation of stored surface heat this tends to be small (Stramma et al., 1986). Secondly, Φ can be either positive or negative at 01:30 LT, although it tends to be only a fraction of its 13:30 LT value due to the supply of energy being relatively small at night compared to the day. This may be less true for areas of land in the height of winter with cloud full days (as we get in Western Europe) and over the sea where significant daytime heat accumulation could in part be re-released as night time latent and sensible heat. Finally, all the terms in Eq. (8) are highly dynamic and yet are treated as constant or varying linearly over the 12 h sample interval. It is difficult to predict what the consequences of this are given it depends on the pattern radiative forcing through the day.

ACPD
10, 14387–14415, 2010

2.3 Satellite datasets

In the present study two different data sources were used for the estimation of R_N and Φ, AIRS and MODIS. The AIRS sounder was carried by the NASA Aqua satellite, which was launched into a sun-synchronous low Earth orbit on 4 May 2002 as part of the NASA Earth Observing System. It gives near global coverage twice daily at 01:30 a.m./p.m. from an altitude of 705 km. AIRS produces 3-dimensional maps of air and surface temperature, water vapor and cloud properties. Level 3 standard monthly day-night data products of air temperature and relative humidity profiles, cloud cover fraction, surface emissivity, near-surface air temperature and surface-skin temperature and columnar total precipitable water at 1°×1° spatial resolution were obtained for 2003 from the online data archive of AIRS, distributed through NASA Mirador data holdings (http://mirador.gsfc.nasa.gov/). The monthly products are simply the arithmetic mean, weighted by counts, of the daily data of each grid box. The multi-day merged products have been used here because the IR retrievals are not cloud proof and the multi-day product gave decent spatial cover in light of missing cloudy sky data. The data products were obtained in hierarchical data format (HDF4) along with their latitude-longitude projection.

We have used the MODIS Aqua atmospheric product datasets (MYD08_D3) (http://modis-atmos.gsfc.nasa.gov/index.html) at 1°×1° spatial resolution for extracting the solar zenith angle field. For generating the surface albedo fields we used narrowband surface reflectances from combined MODIS Terra-Aqua 16 day data (MCD43C4) products acquired from the MODIS data archive (http://ladsweb.nascom.nasa.gov/data/search.html). The native spatial resolution of the MODIS datasets is 0.05°. Therefore, all the narrowband surface reflectances were first resized into 1° by 1° to make them compatible with the AIRS spatial resolution and then the broadband surface albedo was generated from these data.

ACPD
10, 14387–14415, 2010

2.4 Evaluation of R_N and Φ

To evaluate the satellite values of R_N and Φ we have made use of the extensive FLUXNET terrestrial tower network (Baldocchi et al., 2001). Clearly, there is a scale conflict here with the satellite retrievals being 1° whilst the tower observations are for scales of the order of 1 km or less. The tower R_N are from the broadband net radiometer sensors located on each tower. In the absence of reliable measures of G at the tower scale and in order to derive genuinely independent measures of Φ against which to evaluate the satellite data, we have taken the tower net available energy as the sum of the measured sensible and latent heat flux i.e. Eq. (1). Thereby we have assumed that the eddy covariance flux measurements are able to close the energy balance (i.e. $R_N - G = \lambda E + H$), the implications of which will be discussed below. We have chosen 30 sites covering a broad range of geographical locations selected from 7 land cover types including; evergreen broadleaf forest (EBF), mixed forest (MF), evergreen needle forest (ENF), deciduous broadleaf forest (DBF), savanna (SAV), grassland (GRA) and cropland (CRO). A comprehensive list of the site characteristics are provided in Table 1. Each tower evaluation dataset is comprised of the 13:30 LT samples of R_N, H and λE which correspond with the satellite overpass. Again, the evaluation is based on pooling these data into weighted monthly average values. For the evaluation we have elected to compare all 12 months of data for 2003 given this had the best overlap between the FLUXNET and AIRS databases.

3 Results

The locations of the 30 terrestrial evaluation sites are marked in Fig. 1. Figure 2 shows annual average, global satellite scenes for 13:30 LT R_N, c, G and Φ for 2003. Missing data in the images are mainly due to missing data in the AIRS soundings at high latitudes or over the mountain belts where it is difficult to profile air temperature and relative humidity reliably. In addition, persistent cloudy conditions also prevent reliable

ACPD
10, 14387–14415, 2010

retrieval and hence are rejected although these will be less evident in the monthly or annual average data.

Figure 2a shows the global distribution of R_N which generally decreases with latitude as expected. R_N also decreases over land due to the generally higher albedo resulting in reduced absorbtion of the net shortwave radiation (Giambelluca et al., 1997) or relatively higher surface temperature increasing the net longwave component, especially over the drier regions (Liang et al., 1998). As a result the magnitude of R_N was around 200–300 $W m^{-2}$ over the dry desert regions whereas the oceanic values of R_N were 450–700 $W m^{-2}$.

Figure 2b shows the global distribution of c. The oceanic values of 4–8 $MJ m^{-2} K^{-1}$ are equivalent to 1–2 m of sea water, which appears reasonable on the daily time step to which they relate (Stramma et al. 1986). These oceanic values are somewhat noisy due to the small day-night temperature differences observed for the oceans giving a relatively poor signal to noise ratio. However, behind this noise the pattern of oceanic c appears relatively uniform as one might expect. Over land c varies between 0.05–0.5 MJ $m^{-2} K^{-1}$ with wetter tropical and high latitude areas showing significantly higher values than the drier, less vegetated areas as expected. The soil equivalent depth of this heat capacity is approximately 0.01 m, which again appears reasonable for a daily time step (Li and Islam, 1999), although in heavily vegetated areas c is obviously comprised of a more complex aggregation.

Figure 2c shows the global distribution of G. These are the 13:30 LT values, hence them being net positive as an annual average. Between 20° North-South G is approximately 10 to 20% of R_N, and this rises to more than 40% above 50% North-South (Hsieh et al., 2009). Given this opposes the pattern of R_N one would conclude either some deficiencies in the way G is specified here or that R_N partitions into latent heat far more effectively than surface heating in these warm wet environments (Liu et al., 2005). Again, terrestrial values are lower than their oceanic equivalents due in the main to the lower heat capacity as well as reduced R_N as discussed above. This also highlights the role of the vegetation layer in preventing ground heating (Baker and Baker, 2002).

ACPD
10, 14387–14415, 2010

The Sahara appears particularly prominent in this scene with high rates of midday heat accumulation which appears to be associated with a combination of moderate net radiation and relatively high heat capacity. The heterogeneity in this region appears to be related to the pattern of bare darker rock.

Figure 2d shows the global distribution of Φ which follows a similar pattern to R_N as expected, although the pattern of G shown in Fig. 2c dictates that the North-South gradients in Φ are somewhat stronger than those of R_N. Before discussing these results we consider their evaluation. Figure 3a shows the pooled evaluation of R_N which produced an overall correlation of r=0.88(±0.03). Assuming both tower and satellite observations are linearly related through some "true" value, then the pooled values are co-related by R_N(satellite)=0.75(±0.02)R_N(tower)+23.37(±8.20) i.e. a small but significant underestimation in R_N(satellite) relative to R_N(tower). The root mean square deviation (RMSD) between the two was 98 W m^{-2}. The biome specific statistics for R_N are given in Table 2 which reveals correlations ranging between 0.65 (EBF) to 0.96 (ENF), RMSD ranging between 74 (GRA) to 127 W m^{-2} (EBF) and regression statistics ranging between 0.58(±0.08) to 0.87±0.04) for the gain and −32.40(±23.73) to 107.45 (±39.93) for the offset.

Figure 3b shows the evaluation for Φ which produced pooled statistics of r=0.87 (±0.03), Φ(satellite)=0 90(±0.03) Φ(tower)–2.43(±8.19) and RMSD of 72 W m^{-2}. The biome specific statistics for Φ are also given in Table 2 showing correlations ranging from 0.70 (EBF) to 0.95 (ENF), RMSD ranging between 62 (GRA and SAV) to 88 (EBF) W m^{-2} and regression coefficients ranging between 0.66(±0.08) to 1.01(±0.05) and −65.25(±27.07) to 108.71(±32.10) for the gain and offset, respectively.

Figure 4 shows a sample of monthly time series for Φ for both the satellite and the towers. The sites were selected to represent the biome classes considered here and also ones for which complete annual data sets for 2003 were available. These results show the satellite estimates generally track the trends in the tower data and hence the pooled statistics are not masking the within site variability. Again, the site-wise comparative statistics for these data are given in Table 2.

ACPD
10, 14387–14415, 2010

4 Discussion

For R_N the statistics relating the satellite and tower data are comparable with the results of: Bisht et al. (2005) who obtained 74 W m^{-2} RMSD when evaluating MODIS Terra geophysical land products over the Southern Great Plains of the US; Jacobs et al. (2004) who obtained a 12.2% error when evaluating GOES (Geostationary Operational Environmental Satellite) geostationary data over Southern Florida; and Cai et al. (2007) who obtained 13.7% error when evaluating MODIS Terra-Aqua data over China. Stackhouse et al. (2000) evaluated the International Satellite Cloud Climatology Project (ISCCP) data to have errors in the range 10 to 15 W m^{-2} in monthly average shortwave and longwave radiative fluxes. When these errors are compounded in the derivation of R_N and compared with tower data, an RMSD of the order of 98 W m^{-2} appears reasonable.

There have been very few attempts to retrieve satellite estimates of Φ and compare these with ground truth data, although the statistics from our attempt appear to parallel results of Stisen et al. (2008) who studied a single site in the Senegal River basin using 5 km spatial resolution MSG (Meteosat Second Generation) geostationary satellite data and obtained a correlation of 0.51 and an RMSD of 14 to 17% of the mean in comparison to the surface measurements.

As seen in Fig. 3a there is a systematic underestimation of R_N relative to the tower values which exceeds the typical accuracy of net radiometer measurements of 20 W m^{-2} quoted by Foken (2008). We examined this underestimation in more detail by, where possible, evaluating the three individual radiation components of R_N (R_S, $R_{L\downarrow}$ and $R_{L\uparrow}$). All tower sites provided measurements of R_S. Figure 3c shows this is systematically underestimated at the satellite scale with R_S(satellite)= 0.70(±0.02)R_S(tower)+68(±12.24) which could account for the mismatch of R_N(satellite)≈0.75 R_N(tower). Before attempting to account for the various reasons for this underestimation it is important to realise that, unlike the IR components, the shortwave components are all-sky retrievals i.e. like the tower data they do not omit

ACPD
10, 14387–14415, 2010

cloudy sky conditions. As a result, any bias in the shortwave is not as a result of biased sampling when comprising the monthly average. Besides, this would tend to lead to R_S(satellite)>R_S(tower).

There are many possible reasons R_S(satellite)<R_S(tower). Firstly, one has to question the accuracy of Eq. (4). Assuming the measure of cloud cover fraction is accurate, the assumed clear sky transmissivity of 0.75 into Eq. (4) may be too low, although we have avoided any attempt to recalibrate this based on the tower data given it is not clear this is the principle source of the observed bias. Beyond Eq. (4), the diffuse fraction of R_S(tower) can become enriched by surface reflected solar radiation, particularly in undulating terrain (Dubayah and Loechel, 1997). It would also be tempting to implicate nonlinear scaling effects of surface albedo in R_S(satellite)<R_S(tower) (Salomon et al., 2006) because, despite appearing as a linear component in Eq. (3), surface albedo interacts nonlinearly with other dynamic surface variables such as surface wetness and land surface temperature (Ryu et al., 2008) or the leaf area index (Hammerle et al., 2008). However, given the observed bias in R_N appears to be explained through the downwelling shortwave one would conclude that here this effect is of secondary importance.

To probe the specification of R_N further we investigated the individual longwave radiation components in relations to measures of theses fluxes available for a limited subset (14) of tower sites. From Fig. 3d,e it appears that there is quite good agreement between the satellite and tower data for both $R_{L\downarrow}$ and $R_{L\uparrow}$ and that any mismatch is insufficient to explain the discrepancy in R_N. This is somewhat surprising for two reasons. Firstly, unlike the shortwave component, R_L(tower) is all sky whilst R_L(satellite) is only from clear sky conditions where IR retrieval is possible. As a result one would anticipate very significant differences in the monthly average values of the longwave components. However, it is difficult to predict the effect of this biased sampling on R_{NL}(satellite) given cloud interacts with both $R_{L\downarrow}$ and $R_{L\uparrow}$ in complex ways. Secondly, one would anticipate significant scaling effects from the T^4 nonlinearity in Eq. (6) which can result in a disproportionate contribution of warmer elements within the landscape

ACPD
10, 14387–14415, 2010

to both $R_{L\downarrow}$ and $R_{L\uparrow}$ (Kustas and Norman, 2000; Lakshmi and Zehrfuhs, 2002). The fact that these affects are not seen to any significant degree could point to compensating errors in the analysis but does not distract from the central message that of the importance of the bias in the shortwave when accounting for R_N(satellite)<R_N(tower).

Figure 3b and Table 2 show that Φ(satellite)≈0.90Φ(tower) suggesting a slight compensation for the underspecification of R_S through the underspecification of G in the satellite data. However, this evaluation assumes the energy balance to be closed in the tower data (i.e. $R_N - G = \lambda E + H$), which typically is not the case, $\lambda E + H$ often falling short of $R_N - G$ by 20% (Wilson et al., 2002). Because the causes of this energy imbalance remain controversial (see Foken, 2008 for a recent review), it is difficult to estimate how much the tower values of $\lambda E + H$ are actually biased low and hence the extent to which this bias affects our evaluation. By way of illustration, if, in the worst case, the entire energy imbalance was to be attributed exclusively to $\lambda E + H$ (i.e. $R_N - G$ are quantified correctly), then the true midday $\lambda E + H$ could be some 20% greater (Wilson et al., 2002). As a result, the present bias seen in Table 2 would change to Φ(satellite)≈0.72Φ(tower) again implicating R_S as the main source of bias in the satellite retrievals for both R_N and Φ.

5 Conclusions

We have only evaluated the satellite retrievals using data from terrestrial sites, and clearly it would be worthwhile repeating this for the ocean retrievals if possible. We have held back on this evaluation here because of the lack of an extensive network of instantaneous latent and sensible heat flux or radiative flux data over the oceans, although we note that the SEAFLUX project within the Global Energy and Water Experiment (GEWEX) initiative should give rise to such a database in the near future. From the terrestrial evaluation we would argue that the methodology employed here shows some promise for specifying both R_N and Φ, although the results suggests the need for improvements particularly in the specification of R_S. More detailed studies

ACPD
10, 14387–14415, 2010

evaluating the representativeness of each tower site footprint in relation to the 1° scale scene within which it is situated could prove useful in this regard as would methods for cloud-proofing the satellite retrievals under persistent cloudy sky conditions.

Having derived and provisionally evaluated Φ for terrestrial systems this is available to schemes for estimating latent and sensible heat using satellite data. Given we have resorted to the minimal amount of calibration in deriving Φ it would appear sensible if a similar philosophy were adopted in developing satellite-based schemes for these important fluxes. With the availability of high spatial and temporal resolution geostationary imager – sounder suite from GOES and future GIFTS (Geosynchronous Interferometric Fourier Transform Spectrometer) as well as INSAT (Indian National Satellite)-3-D our present approach could be extended to derive Φ at every half hourly time scale.

In addition to opportunities in specifying large scale surface heat and vapour fluxes, the heat capacity estimates made here clearly carry information on variations in terrestrial surface moisture storage and we envisage that studies to develop this concept further could prove fruitful, particularly because of the emergence of satellite microwave data against which the results could be compared.

Acknowledgements. We would also like to acknowledge Goddard Earth Sciences – Data & Information Services Centre (GESS – DISC), Level 1 and Atmosphere Archive and Distribution System (LAADS) web interface, NASA, and for putting the AIRS and MODIS data into the public domain. We kindly acknowledge all the site PI's who are have provided terrestrial flux data through the FLUXNET data archive. The AmeriFlux regional network component of this archive is supported with funding from the US Department Of Environment under its Terrestrial Carbon project.

References

Ammann, C., Flechard, C. R., Leifeld, J., Neftel, A., and Fuhrer, J.: The carbon budget of newly established temperature grassland depends on management intensity, Agr. Ecosyst. Environ., 121, 5–20, 2007.

ACPD

10, 14387–14415, 2010

Anthoni, P. M., Knohl, A., Rebmann, C., Freibauer, A., Mund, M., Ziegler, W., Kolle, O., and Schulze, E. D.: Forest and agricultural land-use-dependent CO_2 exchange in Thuringia, Germany, Glob. Change Biol., 10(12), 2005–2019, 2004.

Aubinet, M., Chermanne, B., Vandenhaute, M., Longdoz, B., Yernaux, M., and Laitat, F.: Long term carbon dioxide exchange above a mixed forest in the Belgian Ardennes, Agr. Forest Meteorol., 108, 293–315, 2001.

Baker, J. M. and Baker, D. G.: Long-term ground heat flux and heat storage at a mid-latitude site, Climatic Change, 54, 295–303, 2002.

Baldocchi, D. D., Falge, E., Gu, L., Olson, R., Hollinger, D., Running, S., Anthoni, P., Bernhofer, C., Davis, K., Evans, R., Fuentes, J., Goldstein, A., Katul, G., Law, B., Lee, X., Malhi, Y., Meyers, T., Munger, W., Oechel, W., Paw U, K. T., Pilegaard, K., Schmid, H. P., Valentini, R., Verma, S., Vesala, T., Wilson, K., and Wofsy, S.: Fluxnet: a new tool to study the temporal and spatial variability of ecosystem-scale carbon dioxide, water vapor, and energy flux densities, B. Am. Meteorol. Soc., 82(11), 2415–3434, 2001.

Baldocchi, D. D., Xu, L. K., and Kiang, N.: How plant functional-type, weather, seasonal drought, and soil physical properties alter water and energy fluxes of an oak-grass savanna and an annual grassland, Agr. Forest Meteorol., 123, 13–39, 2004.

Bastiaanssen, W. G. M., Menenti, M., Feddes, R. A., and Holtslag, A. A. M.: The Surface Energy Balance Algorithm for Land (SEBAL) – Part 1: Formulation, J. Hydrol., 212–213, 198–212, 1998.

Batra, N., Islam, S., Venturini, V., Bisht, G., and Jiang, L.: Estimation and comparison of evapotranspiration from MODIS and AVHRR sensors for clear sky days over the Southern Great Plains, Remote Sens. Environ., 103, 1–15, 2006.

Bisht, G., Venturini, V., Islam, S., and Jiang, L.: Estimation of net radiation using MODIS (Moderate Resolution Imaging Spectroradiometer) data for clear sky days, Remote Sens. Environ., 97, 52–67, 2005.

Cai, G., Xue, Y., Hu, Y., Guo, J., Wang, Y., and Qi, S.: Quantitative study of net radiation from MODIS data in the lower boundary layer in Poyang Lake area of Jiangxi Province, China, Int. J. Remote Sens., 28(19), 4381–4389, 2007.

Cano, D., Monget, J. M., Albuisson, M., Guillard, H., Regas, N., and Wald, L.: A method for the determination of the global solar radiation from meteorological satellite data, Solar Energy, 37, 31–39, 1986.

Carswell, F. E., Costa, A. L., Palheta, M., Malhi, Y., Meir, P., Costa, J. D. R., Ruivo, M. D.,

ACPD

10, 14387–14415, 2010

Leal, L. D. M., Costa, J. M. N., Clement, R. J., and Grace, J.: Seasonality in CO_2 and H_2O flux at an Eastern Amazonian rain forest, J. Geophys. Res.-Atmos., 107(D20), 8076, doi:10.1029/2000JD000284, 2002.

Choudhury, B. J.: Relationships between vegetation indices, radiation absorption, and net photosynthesis evaluated by a sensitivity analysis, Remote Sens. Environ., 22, 209–233, 1987.

Cook, B. D., Davis, K. J., Wang, W., Desai, A., Berger, B. W., Teclaw, R. M., Martin, J. G., Bolstad, P. V., Bakwin, P. S., Yi, C., and Heilman, W.: Carbon exchange and venting anomalies in an upland deciduous forest in Northern Wisconsin, USA, Agr. Forest Meteorol., 126, 271–295, 2004.

de Araújo, A. C., Nobre, A. D., Kruijt, B., Elbers, J. A., Dallarosa, R., Stefani, P., von Randow, C., Manzi, A. O., Culf, A. D., Gash, J. H. C., Valentini, R., and Kabat. P.: Comparative measurements of carbon dioxide fluxes from two nearby towers in a Central Amazonian rainforest: the Manaus LBA site, J. Geophys. Res.-Atmos., 107(D20), 8090, doi:10.1029/2001JD000676, 2002.

Dubayah, R. and Loechel, S.: Modeling topographic solar radiation using GOES data, J. Appl. Meteorol., 36(2), 141–154, 1997.

Fischer, M. L., Billesbach, D. P., Berry, J. A., Riley, W. J., and Torn, M. S.: Spatiotemporal variations in growing season exchanges of CO_2, H_2O, and sensible heat in agricultural fields of the Southern Great Plains, Earth Interact., 11, 1–21, 2007.

Foken, T., Wimmer, F., Mauder, M., Thomas, C., and Liebethal, C.: Some aspects of the energy balance closure problem, Atmos. Chem. Phys., 6, 4395–4402, doi:10.5194/acp-6-4395-2006, 2006.

Foken, T.: The energy balance closure problem: an overview, Ecol. Appl. 18, 1351–1367, 2008.

Gao, W., Coulter, R. L., Lesht, B. M., Qiu, J., and Wesely, M. L.: Estimating clear-sky regional surface fluxes in the Southern Great Plains atmospheric radiation measurement site with ground measurements and satellite observations, J. Appl. Meteorol., 37, 5–22, 1998.

Giambelluca, T. W., Hölscher, D., Bastos, T. X., Frazão, R. R., Nullet, M. A., and Zeigler, A. D.: Observations of albedo and radiation balance over postforest land surfaces in the Eastern Amazon Basin, J. Climate, 10, 919–928, 1997.

Gilmanov, T. G., Soussana, J. F., Aires, L., Allard, V., Ammann, C., Balzarolo, M., Barcza, Z., Bernhofer, C., Campbell, C. L., Cernusca, A., Cescatti, A., Brown, J. C., Dirks, O. M., Dore, S., Eugster, W., Fuhrer, J., Gimeno, C., Gruenwald, T., Haszpra, L., Hensen, A.,

ACPD
10, 14387–14415, 2010

Ibrom, A., Jacobs, A. F. G., Jones, M. B., Lanigan, G., Laurila, T., Ohila, A., Manca, G., Marcolla, B., Nagy, Z., Pilegaard, K., Pinter, K., Pio, C., Raschi, A., Rogiers, N., Sanz, M. J., Stefani, P., Sutton, M., Tuba, Z., Valentini, R., Williams, M. L., and Wohlfahrt, G.: Partitioning European grassland net ecosystem CO_2 exchange into gross primary productivity and ecosystem respiration using light response function analysis, Agr. Ecosyst. Environ., 121(1–2), 93–120, 2007.

Goldstein, A. H., Hultman, N. E., Fracheboud, J. M., Bauer, M. R., Panek, J. A., Xu, M., Qi, Y., Guenther, A. B., and Baugh, W.: Effects of climate variability on the carbon dioxide, water, and sensible heat fluxes above a ponderosa pine plantation in the Sierra Nevada (CA), Agr. Forest Meteorol., 101(2–3), 113–129, 2000.

Gough, C. M., Flower, C. E., Vogel, C. S. Dragoni, D., and Curtis, P. S.: Whole-ecosystem labile carbon production in a north temperate deciduous forest, Agr. Forest Meteorol., 149, 1531–1540, 2009.

Goulden, M. L., Miller, S. D., da Rocha, H. R., Menton, M. C., De Freitas, H. C., Figuera, A. M. E. S., and De Sousa, C. A. D.: Diel and seasonal patterns of tropical forest CO_2 exchange, Ecol. Appl., 14(4), S42–S54, 2004.

Granier, A., Loustau, D., and Breda, N.: A generic model of forest canopy conductance dependent on climate, soil water availability and leaf area index, Ann. Forest Sci., 57(8), 755–765, 2000a.

Granier, A., Biron, P., and Lemoine, D.: Water balance, transpiration and canopy conductance in two beech stands, Agr. Forest Meteorol., 100(4), 291–308, 2000b.

Hammerle, A., Haslwanter, A., Tappeiner, U., Cernusca, A., and Wohlfahrt, G.: Leaf area controls on energy partitioning of a temperate mountain grassland, Biogeosciences, 5, 421–431, doi:10.5194/bg-5-421-2008 2008.

Hildebrandt, A., Aufi, M. A., Amerjeed, M., Shammas, M., and Eltahir, E. A. B.: Ecohydrology of a seasonal cloud forest in Dhofar – Part 1. Field experiment, Water Resour. Res., 43, W10411, doi:10.1029/2006WR005261, 2007.

Hirano, T., Hirata, R., Fujinuma, Y., Saigusa, N., Yamamoto, S., Harazono, Y., Takada, M., Inukai, K., and Inoue, G.: CO_2 and water vapor exchange of a larch forest in Northern Japan, Tellus B-Chem. Phys. Meteorol., 55, 244–257, 2003.

Hirano, T., Segah, H., Harada, T., Limin, S., June, T., Hirata, R., and Osaki, M.: Carbon dioxide balance of a tropical peat swamp forest in Kalimantan, Indonesia, Glob. Change Biol., 13, 412–425, 2007.

ACPD
10, 14387–14415, 2010

Hollinger, D. Y., Goltz, S. M., Davidson, E. A., Lee, J. T., Tu, K., and Valentine, H. T.: Seasonal patterns and environmental control of carbon dioxide and water vapour exchange in an ecotonal boreal forest, Glob. Change Biol., 5(8), 891–902, 1999.

Humes, K. S., Kustas, W. P., and Moran, M. S.: Use of remote sensing and reference site measurements to estimate instantaneous surface energy balance components over a semiarid rangeland watershed, Water Resour. Res., 30, 1363–1373, 1994.

Hutyra, L. R., Munger, J. W., Saleska, S. R., Gottlieb, E., Daube, B. C., Dunn, A. L., Amaral, D. F., de Camargo, P. B., and Wofsy, S. C.: Seasonal controls on the exchange of carbon and water in an Amazonian rain forest, J. Geophys. Res., 112, G03008, doi:10.1029/2006JG000365, 2007.

Hsieh, C. I., Huang, C. W., and Kiely, G.: Long term estimation of soil heat flux by single layer soil temperature, Int. J. Biometeorol., 53, 113–123, 2009.

Jacobs, J. M., Anderson, M. C., Friess, L. C., and Diak, G. R.: Solar radiation, longwave radiation and emergent wetland evapotranspiration estimates from satellite data in Florida, USA, Hydrol. Sci. J., 49, 461–176, 2004.

Jaksic, V., Kiely, G., Albertson, J., Katul, G., and Oren, R.: Net ecosystem exchange of grassland in contrasting wet and dry years, Agric. For. Meteorol., 139(3–4), 323–334, 2006.

Jin, Z., Charlock, T. P., Smith Jr., W. L., and Rutledge, K.: A parameterization of ocean surface albedo, Geophys. Res. Lett., 31, L22301, doi:10.1029/2004GL021180, 2004.

Katul, G. G., Leuning, R., and Oren, R.: Relationship between plant hydraulic and biochemical properties derived from a steady-state coupled water and carbon transport model, Plant Cell Environ., 26(3), 339–350, 2003.

Kustas, W. P., Daughtry, C. S. T., and van Oevelen, P. J.: Analytical treatment of the relationships between soil heat flux/net radiation ratio and vegetation indices, Remote Sens. Environ., 46, 319–330, 1993.

Kustas, W. P. and Norman, J. M.: Evaluating the effects of subpixel heterogeneity on pixel average fluxes, Remote Sens. Environ., 74, 327–342, 2000.

Lakshmi, V. and Zehrfuhs, D.: Normalization and comparison of surface temperatures across a range of scales, IEEE T. Geosci. Remote, 40(12), 2636–2646, 2002.

Li, J. and Islam, S.: On the estimation of soil moisture profile and surface fluxes partitioning from sequential assimilation of surface layer soil moisture, J. Hydrol., 220, 86–103, 1999.

Liang, S., Strahler, A. H., and Walthall, C.: Retrieval of land surface albedo from satellite observations: a simulation study, J. Appl. Meteorol., 38(6), 712–725, 1999.

ACPD

10, 14387–14415, 2010

Liang, X., Wood, E. F., Lettenmaier, D. P., Lohmann, D., Boone, A., Chang, S., Chen, F., Dai, Y., Desborough, C., Dickinson, R. F., Duan, Q., Ek, M., Gusev, Y. M., Habets, F., Irannejad, P., Koster, R., Mitchell, K. E., Nasonova, O. N., Noilhan, J., Schaake, J., Schlosser, A., Shao, Y., Shmakin, A. B., Verseghy, D., Warrach, K., Wetzel, P., Xue, Y., Yang, Z.-L., and Zeng, Q.: The Project for Intercomparison of Land-surface Parameterization Schemes (PILPS) phase 2 (c) Red-Arkansas River basin experiment – Part 2. Spatial and temporal analysis of energy fluxes, Global Planet. Change, 19, 137–159, 1998.

Liu, Z., Vavrus, S., He, F., Wen, N., and Zhong, Y.: Rethinking tropical ocean response to global warming: the enhanced equatorial warming, J. Climate, 18, 4684–4700, 2005.

Ma, Y., Su, Z., Li, Z., Koike, T., and Menenti, M.: Determination of regional net radiation and soil heat flux over a heterogeneous landscape of the Tibetan Plateau, Hydrol. Process., 16, 2963–2971, 2002.

Mallick, K., Bhattacharya, B. K., Rao, V. U. M., Reddy, D. R., Banerjee, S., Hoshali, V., Pandey, V., Kar, G., Mukherjee, J., Vyas, S. P., Gadgil, A. S., and Patel, N. K.: Latent heat flux estimation in clear sky days over Indian agroecosystems using noontime satellite remote sensing data, Agr. Forest Meteorol., 149(10), 1646–1665, 2009.

Mayocchi, C. L. and Bristow, K. L.: Soil surface heat flux: some general questions and comments on measurements, Agr. Forest Meteorol., 75, 43–50, 1995.

Mecikalksi, J. R., Diak, G. R., Anderson, M. C., and Norman, J. M.: Estimating fluxes on continental scales using remotely-sensed data in an atmospheric-land exchange model, J. Appl. Meteorol., 35, 1352–1369, 1999.

Meyers, T. P. and Hollinger, S. E.: An assessment of storage terms in the surface energy balance of maize and soybean, Agr. Forest Meteorol., 125(1–2), 105–115, 2004.

Monteith, J. L.: Evaporation and environment, Symp. Soc. Exp. Biol., 19, 205–234, 1965.

Mu, Q., Heinsch, F. A., Zhao, M., and Running, S. W.: Development of a global evapotranspiration algorithm based on MODIS and global meteorology data, Remote Sens. Environ., 111, 519–536, 2007.

Penman, H. L.: Natural evaporation from open water, bare soil and grass, P. Roy. Soc. Lond., A193, 120–145, 1948.

Pinker, R. T. and Laszlo, I.: Modeling surface solar irradiance for satellite applications on a global scale, J. Appl. Meteorol., 31(2), 194–211, 1992.

Prata, A. J.: A new long-wave formula for estimating downward clear-sky radiation at the surface, Q. J. Roy. Meteor. Soc., 122, 1127–1151, 1996.

ACPD
10, 14387–14415, 2010

Reichstein, M., Tenhunen, J., Roupsard, O., Ourcival, J. M., Rambal, S., Miglietta, F., Peressotti, A., Pecchiari, M., Tirone, G., and Valentini, R.: Inverse modeling of seasonal drought effects on canopy CO_2/H_2O exchange in three Mediterranean ecosystems, J. Geophys. Res.-Atmos., 108(D23), 4726, doi:10.1029/2003JD003430, 2003.

Ryu, Y., Kang, S., Moon, S. K., and Kim, J.: Evaluation of land surface radiation balance derived from moderate resolution imaging spectroradiometer (MODIS) over complex terrain and heterogeneous landscape on clear sky days, Agr. Forest Meteorol., 148, 1538–1552, 2008.

Saigusa, N. Yamamoto, S., Murayama, S., Kondo, H., and Nishimura, N.: Gross primary production and net ecosystem exchange of a cool-temperate deciduous forest estimated by the eddy covariance method, Agr. Forest Meteorol., 112, 203–215, 2002.

Saito, M., Miyata, A., Nagai, H., and Yamada, T.: Seasonal variation of carbon dioxide exchange in rice paddy field in Japan, Agr. Forest Meteorol., 135, 93–109, 2005.

Salomon, J. G., Schaff, C. B., Strahler, A. H., Gao, F., and Jin, Y. F.: Validation of the MODIS bidirectional reflectance distribution function and albedo retrievals using combined observations from the Aqua and Terra platforms, IEEE T. Geosci. Remote, 44(6), 1555–1565, 2006.

Santanello Jr., J. A. and Friedl, M. A.: Diurnal covariation in soil heat flux and net radiation, J. Appl. Meteorol., 42, 851–862, 2003.

Sauer, T. J. and Horton, R.: Soil heat flux, in: Micrometeorology in Agricultural Systems, edited by: Hatfield, J. L., Baker, J. M., American Society of Agronomy, Madison, Wisconsin, USA, 131–154, 2005.

Scholes, R. J., Gureja, N., Giannecchinni, M., Dovie, D., Wilson, B., Davidson, N., Piggott, K., McLoughlin, C., van der Velde, K., Freeman, A., Bradley, S., Smart, R., and Ndala, S.: The environment and vegetation of the flux measurement site near Skukuza, Kruger National Park, Koedoe, 44(1), 73–83, 2001.

Stackhouse, P. W., Gupta, S. K., Cox, S. J., Chiacchio, M., and Mikovitz, J. C.: The WCRP/GEWEX surface radiation budget project release 2: an assessment of surface fluxes at 1° resolution, in: IRS 2000: Current Problems in Atmospheric Radiation, edited by: Smith, W. L. and Timofeyev, Y. M., International Radiation Symposium, St. Petersburg, Russia, 24–29 July, 2000.

Stisen, S., Sandholt, I., Nørgaard, A., Fensholt, R., and Jensen, K. H.: Combining the triangle method with thermal inertia to estimate regional evapotranspiration applied to MSG-SEVIRI data in the Senegal river basin, Remote Sens. Environ., 112, 1242–1255, 2008.

ACPD
10, 14387–14415, 2010

Stramma, L., Cornillon, P., Weller, R. A., Price, J. F., and Briscoe, M. G.: Large diurnal sea surface temperature variability: satellite and in situ measurements, J. Geophys. Res., 16, 827–837, 1986.

Tamai, K., Abe, T., Araki, M., and Ito, H.: Radiation budget, soil heat flux and latent heat flux at the forest floor in warm, temperate mixed forest, Hydrol. Process., 12, 2105–2114, 1998.

Thornton, P. E. and Running, S. W.: An improved algorithm for estimating incident daily solar radiation from measurements of temperature, humidity, and precipitation, Agr. Forest Meteorol., 93, 211–228, 1999.

Urbanski, S., Barford, C., Wofsy, S. Kucharik, C., Pyle, E., Budney, J., Fitzjarrald, D., Czikowsky, M., and Munger, J. W.: Factors controlling CO_2 exchange at harvard forest on hourly to annual time scales, J. Geophys Res., 112, G02020, doi:10.1029/2006JG000293, 2007.

Wielicki, B. A., Barkstrom, B. R., Baum, B. A., Charlock, T. P., Green, R. N., Kratz, D. P., Lee, R. B., Minnis, P., Smith, G. L., Wong, T. M., Young, D. F., Cess, R. D., Coakley, J. A., Crommelynck, D. A. H., Donner, L., Kandel, R., King, M. D., Miller, A. J., Ramanathan, V., Randall, D. A., Stowe, L. L., and Welch, R. M.: Clouds and the Earth's Radiant Energy System (CERES): algorithm overview, IEEE T. Geosci. Remote, 36(4), 1127–1141, 1998.

Wilson, K. B., Goldstein, A. H., Falge, E., Aubinet, M., Baldocchi, D., Berbigier, P., Bernhofer, Ch., Ceulemans, R., Dolman, H., Field, C., Grelle, A., Law, B., Meyers, T., Moncrieff, J., Monson, R., Oechel, W., Tenhunen, J., Valentini, R., and Verma, S.: Energy balance closure at FLUXNET sites, Agr. Forest Meteorol., 113, 223–243, 2002.

Wright, I. R., Gash, J. H. C., da Rocha, R., Shuttleworth, W. J., Nobre, C. A., Maitelli, G. T., Zamparoni, C. A. G. P., and Carvalho, P. R. A.: Dry season micrometeorology of Central Amazonian ranchland, Q. J. Roy. Meteor. Soc., 118, 1083–1099, 1992.

Zhang, J. H., Han, S. J., and Yu, G. R.: Seasonal variation in carbon dioxide exchange over a 200-year-old Chinese broad-leaved Korean pine mixed forest, Agr. Forest Meteorol., 137, 150–165, 2006.

ACPD
10, 14387–14415, 2010

Table 1. Eddy covariance sites used for the evaluation of the satellite derived R_N and Φ.

Biome type	Site name, Country	Latitude	Longitude	Reference
Evergreen broadleaf forest (EBF)	Palagkaraya, Indonasia	−2.35	114.04	Hirano et al. (2007)
	Puechabon, France	43.74	3.6	Reichstein et al. (2003)
	Caxiuana Forest-Almeirim, Brazil	−1.72	−51.46	Carswell et al. (2002)
	Manaus – ZF2 K34, Brazil	−2.61	−60.21	de Araújo et al. (2004)
	Santarem-Km67, Brazil	−2.86	−54.96	Hutyra et al. (2007)
	Santarem-Km83, Brazil	−3.02	−54.58	Goulden et al. (2004)
Mixed forest (MF)	Vielsalm, Belgium	50.31	5.99	Aubinet et al. (2001)
	Tomakomai National forest, Japan	42.73	141.52	Hirano et al. (2003)
	Changbaishan, China	42.4	128.09	Zhang et al. (2006)
Grassland (GRA)	Oensingen1 grass, Switzerland	47.29	7.73	Ammann et al. (2007)
	Neustift/Stubai Valley, Austria	47.12	11.32	Hammerle et al. (2008)
	Goodwin Creek, USA	34.25	−89.87	Unpublished
	Bugacpuszta, Hungary	46.69	19.61	Gilmanov et al. (2007)
	Dripsey, Ireland	51.99	−8.75	Jaksic et al. (2006)
Cropland (CRO)	ARM Southern Great Plains, USA	36.61	−97.49	Fischer et al. (2007)
	Bondville, USA	40.01	88.29	Meyers et al. (2004)
	Tsukuba, Japan	36.05	140.03	Saito et al. (2005)
Evergreen needleleaf forest (ENF)	Le Bray, France	44.72	−0.77	Granier et al. (2000a)
	Duke Forest – loblolly pine, USA	35.98	−79.09	Katul et al. (2003)
	Blodgett forest, USA	38.89	−120.63	Goldstein et al. (2000)
	Howland forest, USA	45.2	−68.74	Hollinger et al. (1999)
Deciduous broadleaf forest (DBF)	Harvard Forest EMS Tower (HFR1), USA	42.54	−72.17	Urbanski et al. (2007)
	Univ. of Michigan Biological Station, USA	45.56	−84.71	Gough et al. (2009)
	Willow Creek, USA	45.81	−90.08	Cook et al. (2004)
	Hesse Forest-Sarrebourg, France	48.67	7.06	Granier et al. (2000b)
	Hainich, Germany	51.08	10.45	Anthoni et al. (2004)
	Morgan Monroe State forest, USA	39.32	−86.41	Baldocchi et al. (2001)
	Takayama, Japan	36.15	137.42	Saigusa et al. (2002)
Savanna (SAV)	Tonzi Ranch, USA	38.43	−120.97	Baldocchi et al. (2004)
	Skukuza, South Africa	−25.02	31.49	Scholes et al. (2001)

ACPD
10, 14387–14415, 2010

Table 2. Comparative statistics for the satellite and tower derived R_N and Φ for a range of biomes. Values in the parenthesis are one standard deviation except for the correlation (r) where the values in the parenthesis are the standard errors of r.

Biome	R_N RMSD (Wm^{-2})	Gain	Offset	r	N	Φ RMSD (Wm^{-2})	Gain	Offset	r	N
EBF	126.67	0.58 (±0.08)	107.45 (±39.93)	0.65 (±0.09)	69	87.67	0.66 (±0.08)	108.71 (±32.10)	0.70 (±0.09)	65
MF	104.21	0.82 (±0.07)	−32.40 (±23.73)	0.89 (±0.08)	36	87.29	0.97 (±0.10)	−65.25 (±27.07)	0.86 (±0.09)	32
GRA	74.29	0.73 (±0.05)	51.37 (±15.88)	0.88 (±0.06)	59	61.51	0.83 (±0.07)	15.71 (±16.21)	0.86 (±0.07)	53
CRO	89.13	0.73 (±0.08)	35.62 (±28.57)	0.84 (±0.09)	36	53.31	0.99 (±0.10)	−0.23 (±23.98)	0.87 (±0.09)	36
ENF	85.45	0.87 (±0.04)	−26.83 (±14.78)	0.96) (±0.04)	48	66.7	1.01 (±0.05)	−56.56 (±15.27)	0.95 (±0.05)	46 46
DBF	92.77	0.71 (±0.05)	21.74 (±15.15)	0.85 (±0.06)	84	71.57	0.88 (±0.06)	−16.70 (±14.23)	0.85 (±0.06)	80
SAV	103.98	0.69 (±0.08)	56.28 (±36.08)	0.87 (±0.11)	23	61.98	0.97 (±0.11)	−14.42 (±37.68)	0.88 (±0.25)	23
Pooled	98.21	0.75 (±0.02)	23.37 (±8.20)	0.88 (±0.03)	355	72.26	0.90 (±0.03)	−2.43 (±8.19)	0.87 (±0.03)	335

EBF=Evergreen broadleaf forest, MF=Mixed forest, GRA=Grassland, CRO=Cropland, ENF=Evergreen needleleaf forest, DBF=Deciduous broadleaf forest, SAV=Savanna

ACPD
10, 14387–14415, 2010

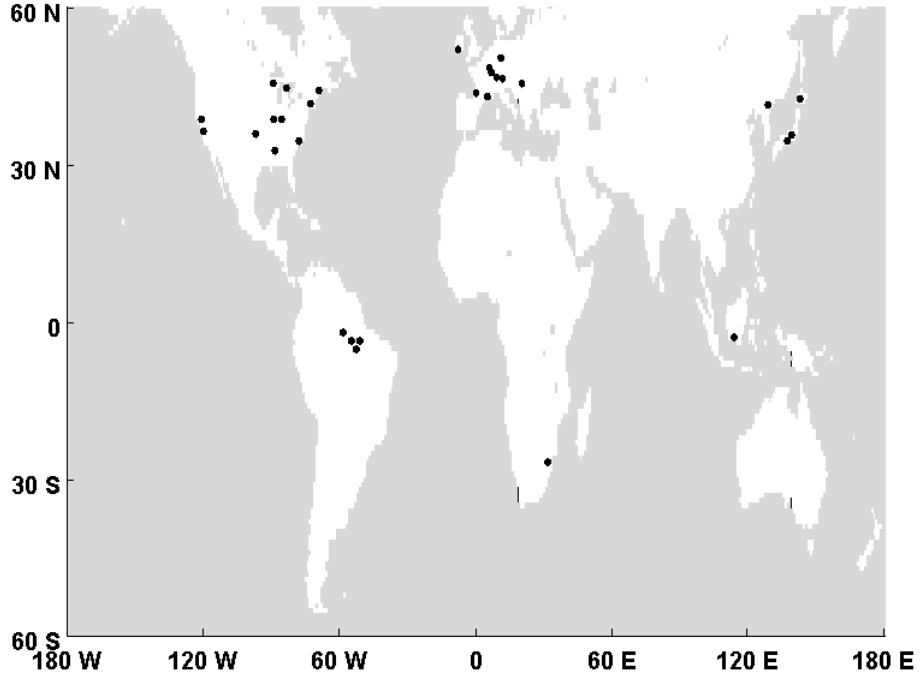

Fig. 1. The distribution of the 30 eddy covariance tower sites used for evaluating R_N and Φ.

ACPD
10, 14387–14415, 2010

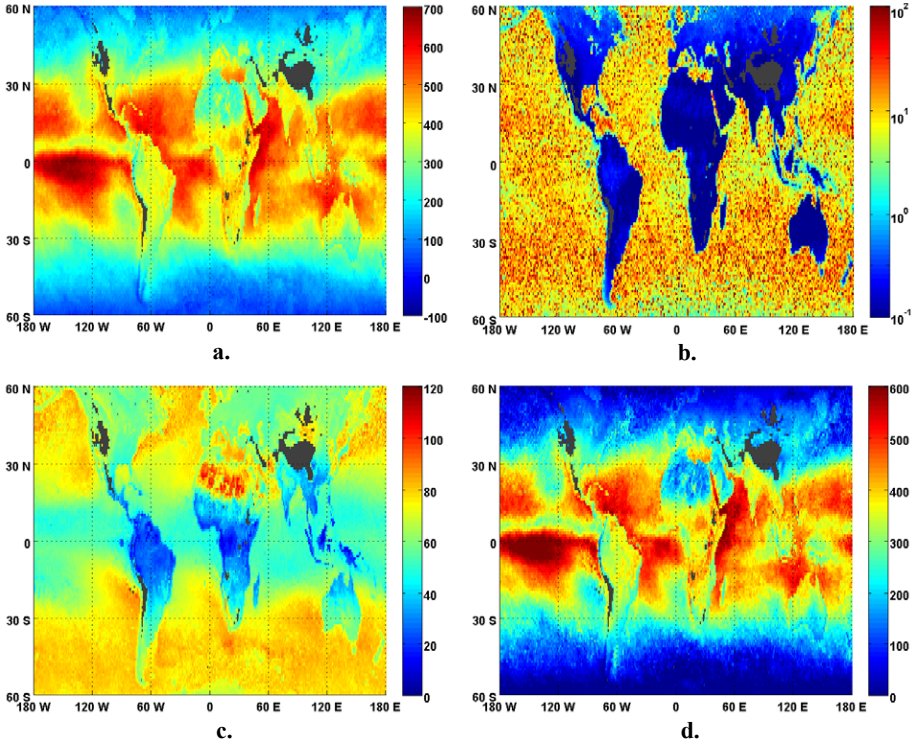

Fig. 2. Global fields for annual average 13:30 LT: **(a)** net radiation R_N (W m^{-2}); **(b)** surface heat capacity, c (MJ m^{-2} K^{-1}); **(c)** surface heat accumulation rate, G (W m^{-2}); **(d)** net available energy, Φ (W m^{-2}), for 2003.

ACPD
10, 14387–14415, 2010

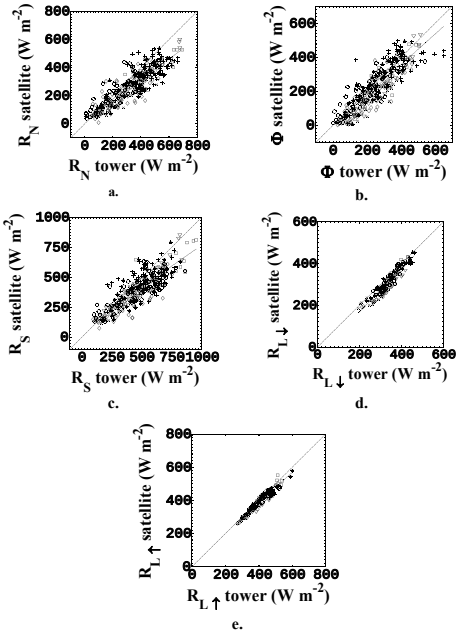

Fig. 3. Comparison of satellite and tower monthly average 13:30 LT **(a)** R_N and **(b)** Φ. For details of the site characteristics see Table 1. For the comparative statistics see Table 2. The solid line is the pooled linear regression given in Table 2. Comparison of satellite and tower monthly average 13:30 LT **(c)** R_S, **(d)** $R_{L\downarrow}$ and **(e)** $R_{L\uparrow}$ for a selection of sites for which tower data for R_S (360 data points), $R_{L\downarrow}$ (159 data points) and $R_{L\uparrow}$ (159 data points) were available. The linear fit (solid line) between the two sources of R_S is, R_S(AIRS)=0.70(±0.02)R_S(tower)+67.68(±12.24); r=0.84(±0.03). The linear fit (solid line) between the two sources of $R_{L\downarrow}$ is, $R_{L\downarrow}$(AIRS)= 1.03(±0.03)$R_{L\downarrow}$(tower)−36.91(±10.05); r=0.95(±0.03). The linear fit (solid line) between the two sources of $R_{L\uparrow}$ is, $R_{L\uparrow}$(AIRS)=0 91(±0.02) $R_{L\uparrow}$(tower)+20.43(±8.77); r=0.96(±0.02). The dashed lines are 1:1 in all cases. (+ EBF; x MF; ∘ GRA; ∗ CRO; ∇ ENF; ◇ DBF; □ SAV).

ACPD
10, 14387–14415, 2010

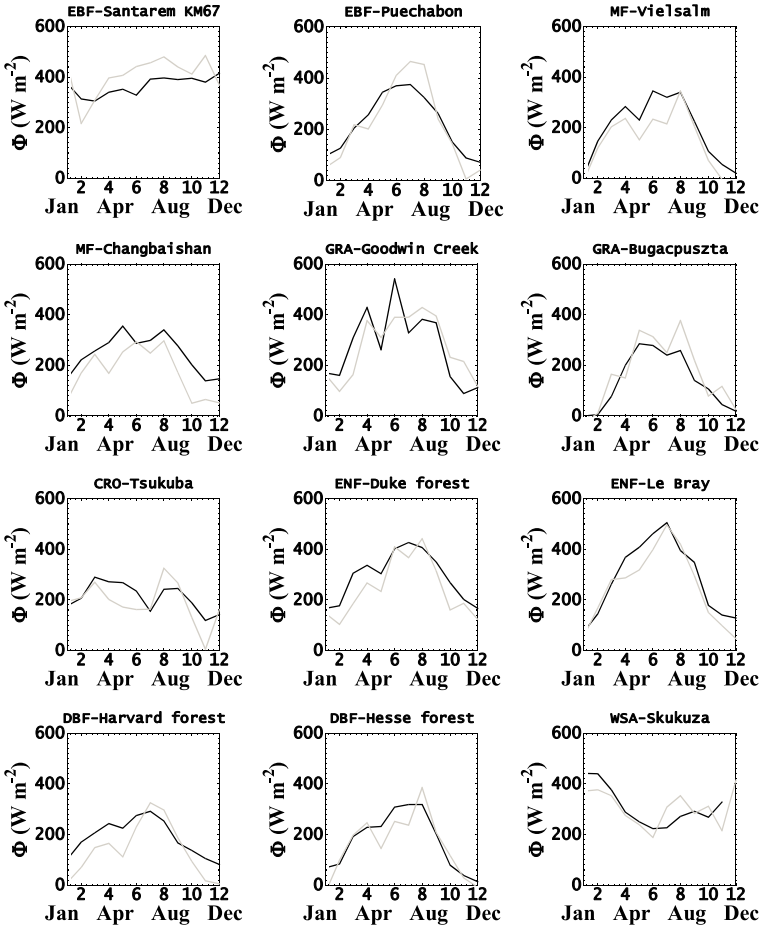

Fig. 4. Satellite (grey) and tower (black) time series of monthly average 13:30 LT net available energy Φ for a selection of sites for 2003.

ACPD
10, 14387–14415, 2010